RSC Advances

ROYAL SOCIETY OF CHEMISTRY

www.rsc.org/advances

Graphical Abstract

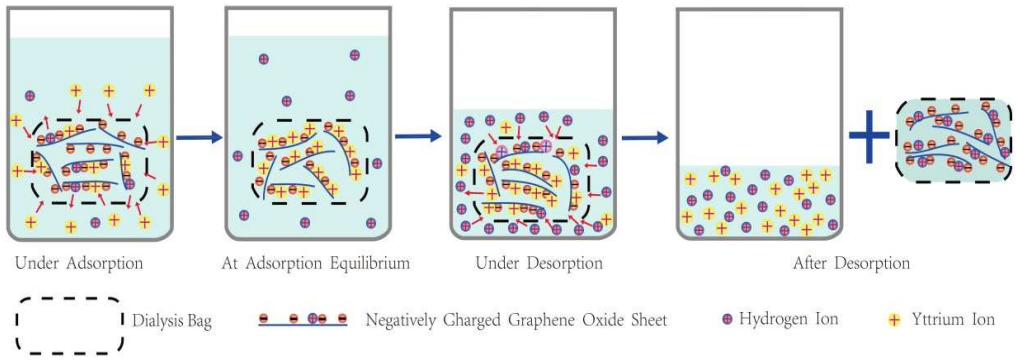

Schematic diagram of Y(III) adsorption and desorption on graphene oxide (GO) nanosheets in colloidal suspensions loaded in dialysis bag.

Reusable Colloidal Graphene Oxide Suspensions Combined with Dialysis Bag for Recovery of Trace Y(III) from Aqueous Solutions†

Weifan Chen, [a, b,*] Linlin Wang, [a] Mingpeng Zhuo, [a] Yiping Wang, [a] Sulei Fu, [a] Yongxiu Li, [b] and Shilin Wu [c]

Abstract Recycling trace rare earth elements (REEs) from effluents from mine and refinery is vital for the protection of global environment and utilization of valuable REE resource. In this work, a novel and highly efficient method for second-pollution-free adsorptive recovery of trace Y(III) from aqueous solutions by colloidal graphene oxide (GO) suspensions loaded in dialysis bag has been developed based on the properties of GO suspensions and the sieving characteristics of dialysis membrane. The effects of pH, ionic strength and temperature on Y(III) adsorption/desorption on GO were studied. The thermodynamics and kinetics investigations on Y(III) adsorption on GO were also conducted. The maximum adsorption capacity of Y(III) on GO at pH=5.9±0.1 and T=303 K was 190.48 mg·g^{-1}, higher than any other adsorbents reported so far. In the fourth consecutive adsorption-desorption cycles, the Y(III)-saturated GO suspension was still able to resume colloidal state in pH=0.9 HNO_3 aqueous solution with a desorption rate of 74.26% in the fourth adsorption-desorption cycle while the regenerated GO maintains the adsorption capacity of 138.73 mg·g^{-1}. The adsorption/desorption capacities of Y(III) on GO depended more on pH than on ionic strength and temperature. The studies on adsorption thermodynamics and kinetics showed that the adsorption of Y(III) on GO was an endothermic, spontaneous and monolayer absorption process,

and perfectly fitted the Langmuir model and the pseudo-second-order model. In summary, GO is a highly efficient and easily reusable adsorbent with promising application for the treatment of industrial wastewater and the enrichment and recovery of lanthanide. More importantly, the combination of colloidal GO suspension with dialysis membrane facilely avoids the re-pollution of the treated solutions, drastically reduces workload in separation and recovery of GO and provides an alternative route for actual application of nano-sized adsorbents in environmental pollutant removal and valuable resource recovery from wastewater.

[a]*School of Materials Science & Engineering, Nanchang University, Nanchang 330031, PR China; E-mail: weifan-chen@163.com; Fax: +86 079183969329; Tel.: +86 079183969553*

[b]*Research Center of Rare Earths & Micro/Nano Functional Materials, Nanchang University, Nanchang 330031, PR China*

[c]*School of Environmental & Chemical Engineering, Nanchang University, Nanchang 330031, PR China*

[†]*Electronic supplementary information (ESI) available.*

1. Introduction

Over the past three decades, global reserves of REEs have been declining quickly and drastically growing REEs have been released into the environment and exposed to humans owing to more and more widespread use of rare earths elements (REEs) in high-technology industries. [1] Especially in the surrounding areas of weathered crust elution-deposited rare earth mine and REE refinery in southern China, effluents from *in-situ* leaching mining and indiscriminate discharge of industrial wastewater not only pollute severely surface water and ground water, threaten health of the local inhabitants, but also cause huge loss of ionic state REEs.[2] Although REEs concentrations in these wastewater are as low as one to hundreds of mg L^{-1}, more than 7.2 million tons of such wastewater are generated and discharged annually due to lack of effective recovery techniques.[3] Hence, highly efficient enrichment and recovery of REEs from wastewater is an urgent task for the protection of human health and environment as well as full utilization of REE resources.

Various methods for the recovery and removal of REE ions from the wastewater have been developed, including adsorption [4], membrane separation [5], precipitation [6], etc. Among these techniques, adsorption is regarded as a simple, economic and efficient approach especially for the separation of trace REE ions. [7, 8]It is reported that, such absorbents as by-pass cement dust [4], activated carbon [9], γ-Al_2O_3 [10], bacterial cell walls [11], and polyethyleneglycol (phosphor-molybdate and tungstate) heteropolyacid [12], etc. could be applied in the removal of REE ions from water.

In the past decade, graphene, a newly emerging two-dimensional nanomaterial

has attracted enormous scientific interests of worldwide researchers and promises potential applications in a variety of areas owing to a range of unique and prominent properties, Application of graphene, chemically modified graphene and graphene-based nanocomposites in environmental clearup, has been one of the hot spots in present research. [13] In addition to high specific surface area, GO is the most common chemically modified graphene with a range of abundant oxygen-containing functional groups, such as epoxide, hydroxyl, carbonyl and carboxyl groups, which makes it hydrophilic and easily disperse in water to form stable colloidal suspensions. [14, 15] GO can be readily prepared by the well-established modified Hummers method using common flake graphite as raw material on an industrial scale and at an economic cost in the near future. Therefore, GO has become an ideal adsorbent in the removal of metal ions and organic pollutants from aqueous solution. It was documented that GO had a higher adsorption capacity than any of today's adsorbents in the removal of Cu(II) [16], Zn(II) [16], Cd(II) [16,17], Co(II) [17], Pb(II) [17,18] , U(VI) [19], Eu(III) [20] and Th(IV) [21] from water. To enhance their adsorption properties for metal ions, numerous graphene-based nanocomposites have been synthesized by chemical modification of GO or attachment of nanoparticles on GO [22-25] However, as graphene-based adsorbents are usually dispersed into wastewater and form a stable colloid when used in the wastewater treatment, a few troublesome problems restricting their application in real work has been confronting us, i.e. difficult sedimentation and separation of the nanoadsorbents and huge filtration volume in their recovery and separation from the treated wastewater after the adsorption process as well as regeneration of the

nanoadsorbents. If not solved properly, the re-pollution of the treated solutions will occur in and the cost of industrial applications will be increased. [26]

To separate GO from the treated wastewater quickly and avoid the re-pollution, major investigations have been focused on synthesis of magnetite/GO nano-composites by attaching magnetite nanoparticles on GO on the basis of the convenient magnetic separation. [24-29] Nevertheless, the attachment of magnetite nanoparticles on GO inevitably lessens unit weight absorption capacity due to adding dead weight, [24] which is also confirmed by comparing data in the references. [16, 29] It can be due to the fact that the nanoparticles may instead tie up adsorption sites, limiting adsorption capacity. Furthermore, the large-scale application of magnetic nanoparticles/graphene oxide hybrids in removing organic ion and inorganic pollutants in wastewater is still restricted by synthetic complexity and high cost of the functional hybrids. In particular, the magnetic nanoparticles on the surface of GO tend to dissolve in strong acidic solutions, which greatly limits their application. [27]

In the present work, we have proposed a facile and general strategy for adsorptive recovery of trace metal ions from wastewater by combining colloidal GO suspension with dialysis membrane, which promises widespread application in water purification and resource recycling due to no re-pollution of the treated solutions, convenient nanoadsorbent separation, and great reduction in separation workload and application cost. Taking Y(III) as the representative REE, which is the richest REE in the weathered crust elution-deposited rare earth mine in south China, the objectives of this study are to (a) test and verify the adsorptive recovery feasibility of trace Y(III)

from aqueous solutions, using colloidal aqueous suspensions of GO loaded in dialysis bags; (b) study the effects of pH, ionic strength and temperature on Y(III) adsorption/desorption; (c) investigate the regenerability and reusability of Y(III)-saturated GO; (d) deal with the thermodynamics and kinetics of Y(III) adsorption on colloidal GO.

2. Experimental

2.1 Materials

BIOSHARP regenerated cellulose dialysis bags with 8000~14000 in molecular weight cut-off and 21 mm in diameter were purchased from Shanghai treasure biological technology co., LTD and used after pretreatment in boiling deionized water for 3~5 min.

Colloidal GO suspension was synthesized using modified Hummer method from the flake graphite (purity: 99.95wt%, particle size: 325 meshes, Xianfeng nano Co., Ltd.). Briefly, flake graphite was strongly oxidized by using $KMnO_4$ and concentrated H_2SO_4 under ultrasonication, and H_2O_2 was then added to eliminate the excess MnO_4^- anions. Subsequently, the purification processes such as rinse with deionized water, centrifugal separation, ultrasonication and BIOSHARP membrane dialysis were repeated until the deionized water for dialysis was neutral, thus the stock suspension of GO was obtained, whose concentration was determined by gravimetric method. The GO suspensions for ion adsorption were prepared by diluting according to the experimental requirements. The Y(III) aqueous standard solution at 12 $mg \cdot L^{-1}$ was prepared by dissolving Y_2O_3 (purity 99.999 wt%) in nitric acid and followed by

heating until the excessive nitric acid was evaporated. The detailed processes are described in the Supporting Information

2.2 Characterization of GO

Graphene oxide were characterized by transmission electron microscopy (TEM), atomic force microscopy (AFM), powder X-ray diffraction (XRD), Raman spectroscopy and Fourier transformed infrared spectra (FT-IR). The TEM image was obtained by a JEOL transmission electron microscope (JEM-2100, Japan). The AFM image was obtained in air using a Digital Instrumental Nanoscope III in tapping mode. The XRD patterns were measured using an Advance D8 diffractometer with Cu-Kα radiation. The Raman spectrum was recorded with a JobinYvon Lab Ram HR800 spectroscopy at room temperature. The FT-IR spectroscopy measurement was conducted by using a Nicolet 5700 spectrometer in KBr pellet. The zeta potentials of 100 $mg \cdot L^{-1}$ colloidal aqueous GO suspensions as a function of pH were measured by a Zetatrac dynamic light scattering detector (Microtrac Limited Corp., USA) at 303 K.

2.3 Batch Adsorption experiments

In the adsorption experiment, 10 ml 100 $mg \cdot L^{-1}$ pH=5.9±0.1 colloidal GO suspension was sealed into a dialysis bag to constitute an adsorption unit. The batch adsorption experiments of Y(III) on GO nanosheets in colloidal suspensions were carried out by immersing an adsorption unit in 25 ml 12 $mg \cdot L^{-1}$ Y(III) aqueous solutions in a large-mouth conical flask placed in a water-bathing thermostatic shaker. Two aliquot parts of the treated solutions were sampled at regular intervals to determine Y(III) concentrations by visible adsorption spectrophotometric method

using arsenazo-III as the chromogenic agent at the wavelength of 656 nm. The average of duplicate determinations with the relative errors below 5% was the Y(III) concentration of the treated solution. The amounts of Y(III) adsorbed by the colloidal GO suspensions were calculated from the differences between the initial concentration (C_0, mg·L^{-1}) and equilibrium one (C_e, mg·L^{-1}).

Adsorption capacity: $q_e=[(V_s \cdot C_0-(V_s+V_g) \cdot C_e]/M$

Where q_e is the equilibrium adsorption capacity of Y(III) on the GO (mg·g^{-1}), V_s and V_g are the volumes of the treated solution and colloidal GO suspension (L), respectively, and M is the mass of the GO (g).

As pH of the common wastewater from RE mine and refinery is usually about 6.0, all the adsorption experiments were conducted at 303 K, using the pH=5.9±0.1 Y(III) solution and GO suspension in dialysis bag unless specified otherwise. For the experiments of pH effect, the initial pH of Y(III) aqueous solution to be treated was adjusted to be in the range of 2.0~11.0 by adding negligible volume of 0.1 or 0.05 mol·L^{-1}HNO_3 or NaOH solution. It was noted that pH of the Y(III) solution was ＜7.86 during the absorption process. and that no Y(III) precipitation occurred in the aqueous solution For the experiments of ionic strength effect, $NaClO_4$ was added to achieve the Y(III) solutions containing the desired $NaClO_4$ concentrations.

2.4 Desorption and regeneration study

For the desorption study, 10 ml 100 mg·L^{-1} pH=5.9±0.1 colloidal GO suspension was sealed into a dialysis bag to constitute an adsorption unit. Then the adsorption unit was immersed into 25 ml of Y(III) solutions with initial concentration of 12.0

$mg \cdot L^{-1}$, and was kept in a water-bathing thermostatic shaker at 303 K for 25 min. Two aliquot parts of each treated solution were sampled to determine Y(III) concentrations. Finally, Y(III)-saturated adsorption units were soaked into 25 ml of 0.1 M HNO_3 aqueous solutions, respectively, and vibrated for 60 min. After desorption, two aliquot parts of each treated solution were sampled to determine Y(III) concentrations, using spectrophotometric determination method. The desorption capacity and desorption rate of Y(III)-saturated GO were calculated according to the following equations:

Desorption rate: $R_d = V_d C_d / q_e M$

Where C_d is the concentrations of Y(III) in the desorption solution ($mg \cdot L^{-1}$), M is the mass of the GO (g) , V_d and V_s are the volumes of the desorption solution and Y(III)-saturated GO suspension (L), respectively, and q_e is the equilibrium adsorption capacity of Y(III) on the GO ($mg \cdot g^{-1}$), which is calculated by the following equation: $q_e = [(V_s \cdot C_0 - (V_s + V_g) \cdot C_e]/M$.

3. Results and discussion

3.1 Characterization of GO

TEM, AFM, XRD, Raman and FT-IR characterization of the prepared GO nanosheets, and pH dependent Zeta potentials of the colloidal GO suspensions are presented in Fig. 1. The TEM image in Fig. 1a shows that crumpled flower-like GO nanosheets are formed, where thetransparent areas indicate few-layer GO and the dark areas suggest the crumpled section of GO. From the AFM image in Fig. 1b, the GO nanosheets are in micrometer scale in lateral dimensions and about 0.947 nm in thickness, suggesting that the presence of one-layered GO nanosheets. The thickness

of one layer GO nanosheet is 0.8~1.0 nm. [30]

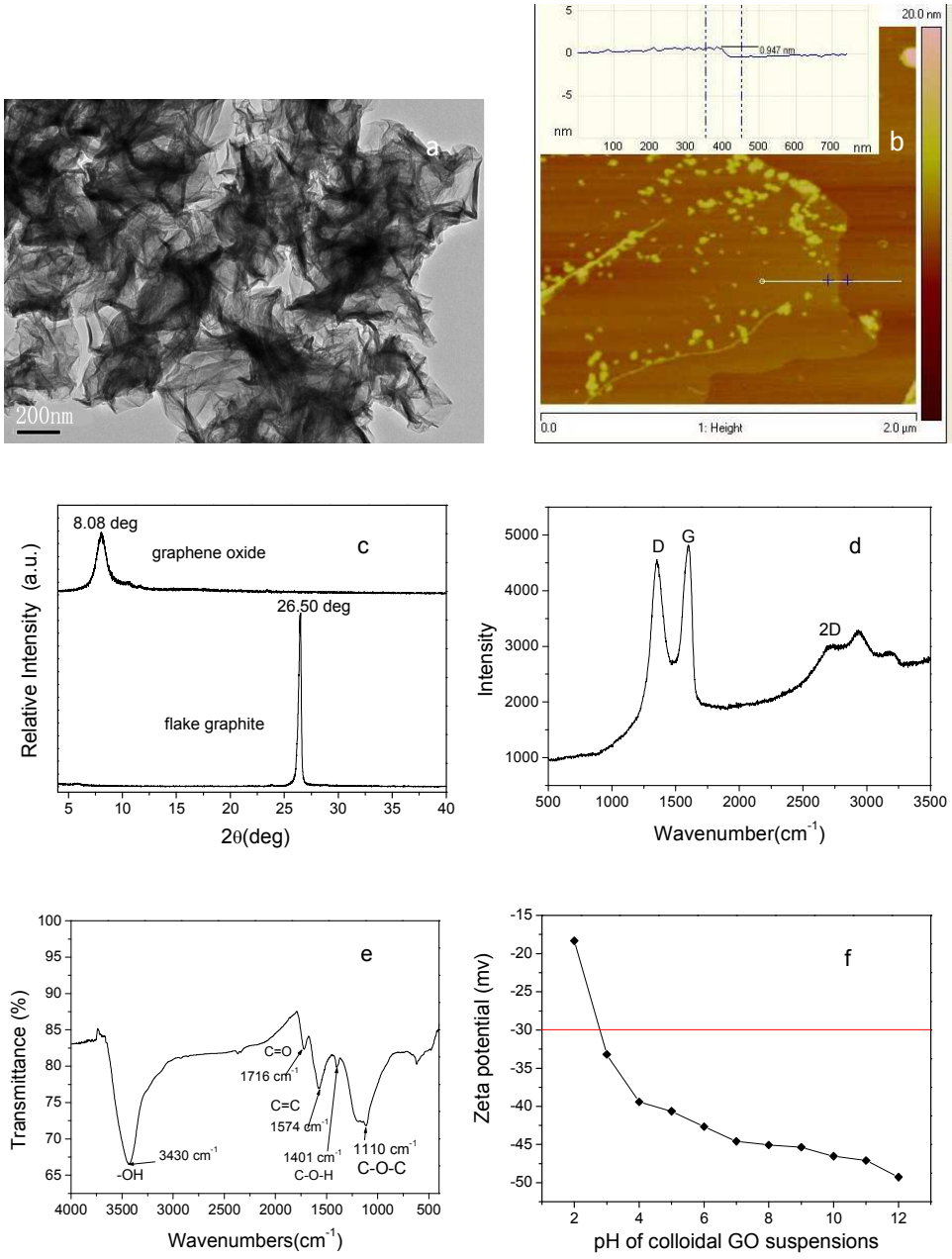

Fig. 1. Characterization of GO nanosheets: (a) TEM image, (b) AFM image with a representative height profile; (c) XRD patterns of flake graphite and GO nanosheets; (d) Raman spectrum; (e) FT-IR spectrum; (f) Zeta potentials of 100 mg·L^{-1} colloidal GO suspensions as a function of pH.

Fig. 1c presents XRD patterns of GO nanosheets and flake graphite, As Fig. 1c

shows, the intense diffraction peak at 2θ=26.40° (d=0.335 nm) corresponding to the natural graphite spacing (002) of graphite plane disappears in the GO nanosheets while the relatively weak diffraction peak attributed to the (001) reflection of GO appears at around 2θ=8.07° (d=0.940 nm), lower than the reported diffraction angles due to the higher oxidation degree of GO. [31, 32] Owing to the introduction of abundant oxygen-containing functional groups on the graphite sheets, the interlayer spacing increases from 0.335 nm of pristine graphite to 0.940 nm of the GO, which coincides well with the AFM measurement (0.947 nm). [33]

In the Raman spectrum(Fig. 1e), the G band at~1580 cm^{-1} is attribute to the vibration of sp^2 carbon atoms in a graphitic 2D hexagonal lattice, and the D band at~1350 cm^{-1} is associated to the vibrations of sp^3 carbon atoms of defects and disorder. The weak and broad 2D peak at ~ 2700 cm^{-1} is assigned to the indication of disorder as the result of an out-of-plane vibration mode. These strong G, D, and 2D bands are in good agreement with previous results of GO characterization. [34]

To identify the functional groups on the surfaces of the GO nanosheets, FT-IR spectrum was recoded. As shown in Fig. 1e, the characteristic absorption peaks of several oxygen-containing groups are observed, including the broad and intense peak of O-H groups centered at 3430 cm^{-1}, the strong C–O–C peak around 1100 cm^{-1}, the 1401 cm^{-1} peak arising from the bending vibration of C–O–H groups, and the peaks at 1716 $cm^{-1}$and 1574 cm^{-1}, corresponding to the C=O and C=C, respectively, which suggests that large amounts of oxygen-containing functional groups (hydroxyl, carboxyl, carbonyl, and epoxy groups) are present on the surface of GO.

As presented in Fig. 1f, in the pH range from 2 to 11, all the zeta potentials of as-prepared colloidal GO suspensions are negative, and becomes more negative with increasing pH value, indicating that these GO sheets are highly negatively charged when dispersed in water and become more stable in more basic solution. The results are consistent with the previous report. [15]

3.2 Effect of pH, ionic strength and temperature on adsorption/desorption of Y(III) on GO nanosheets

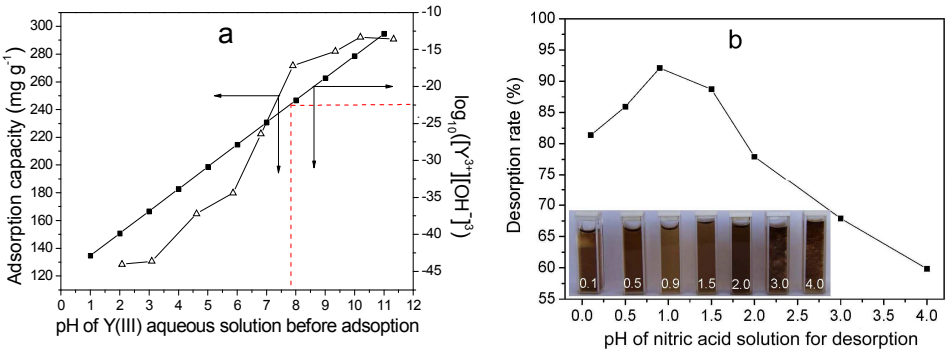

Fig. 2. (a) Effect of pH on the adsorption of Y(III) on GO nanosheets in colloidal suspensions and $\log_{10}[Y^{3+}][OH^-]^3$ curve of the Y(III) solution to be adsorbed as a function of pH (T = 313 K, adsorption time:25 min, C_{GO}=100 mg·L^{-1}, V_{GO}=10 mL, C[Y(III)]$_{initial}$ =12 mg·L^{-1}, V[Y(III)]=25 mL). The vertical line indicates the onset pH of Y(III) precipitation from the C[Y(III)]$_{initial}$ =12 mg·L^{-1}solution; (b) Effect of pH of HNO_3 solution on the desorption of Y(III) on GO nanosheets in colloidal suspensions (pH= 0.9, V_{HNO3} =25 ml, desorption time: 60 min). The inset is photo of GO suspensions after desorption in nitric acid solutions with different pH.

In Fig. 2a, the adsorption curve of Y(III) on GO nanosheets in colloidal suspensions as a function of Y(III) solution pH is presented by the open triangular dot line and $\log_{10}[Y^{3+}][OH^-]^3$ curve of the Y(III) solution to be adsorbed as a function of pH is displayed by the filled square dot line. The adsorption capacity of Y(III) on GO nanosheets increases slowly at pH < 6, quickly at pH 6~ and then maintains over 270

mg g^{-1} with lower growth rate at pH > 8. From the results in Fig. 1f, all the zeta potentials of colloidal GO suspensions in the pH range from 2 to 11 are negative, and become more negative with increasing pH value, which is due to different degrees of ionization of the carboxylic acid and phenolic hydroxyl groups on the GO nanosheets as a function of pH value. The positive metal ions tend to be adsorbed on the negatively-charged surface of GO nanosheets owing to the electrostatic attraction. With increasing pH value, the zeta potentials are more negative and the electrostatic interactions between Y(III) and GO nanosheets become stronger, and thereby the enhanced Y(III) adsorption is resulted in. At lower pH values, part of negatively-charged functional groups are protonated with H^+, and the bulk binding sites are occupied, so the GO adsorption capacity for Y(III) decreased. According to the logarithmic value of precipitation constant $\log_{10}K_{sp}[Y(OH)_3] = -22.76$，it can be calculated from Fig. 2a that for $C_{[Y(III)]} = 20$ mg·L^{-1} aqueous solution, Y(III) begins to form precipitation at pH≥7.86 in the absence of 10 ml colloidal GO suspension with pH=5.9±0.1. The experimental results showed that pH value of the pH=11 solution after GO adsorption fell to 7.60, which is below the pH value of Y(III) precipitation (7.86). Therefore, when 10 ml 100 mg·L^{-1}pH=5.9±0.1GO suspension in dialysis bag is used for treatment of Y(III) solutions with the pH ranging from 2.0 to11.0, for Y(III) solutions with pH<7.86, most Y(III) ions are directly adsorbed by GO. For Y(III) solutions with pH≥7.86, the formed Y(III) precipitates dissolve gradually into Y(III) ions in the adsorption process, which are rapidly adsorbed by GO through micropores of dialysis membrane

Fig. 2b shows that effect of pH of nitric acid solution on the desorption behavior of Y(III) on GO nanosheets in colloidal suspensions and the photo of GO suspensions after desorption in nitric acid solutions with different pH. As pH of nitric acid solution for desorption varies from 0.1 to 4.0, the desorption rate of Y(III) on GO nanosheets increases at start and then decreases, achieving peak value of 93% at pH= 0.9, which does not coincide with the common belief that more acidic the desorption solution is, the higher the desorption. From the inset image of Fig. 2b, it can be seen that pH value of nitric acid solution for desorption has great influence on the dispersion state of GO suspension after desorption. More significantly, it can be found that the desorption rate has an obvious correlation with the agglomeration extent of regenerated GO suspension. As demonstrated in Fig. 2b, the GO after desorption almost resumes the initial colloid state and shows highest desorption rate at pH 0.9. Moreover, the darker and more aggregated GO suspension after desorption is, the lower the corresponding desorption rate of Y(III) on GO nanosheets is. When GO suspension is regenerated in desorption solution at very low pH, the high concentration of H^+ may result in the restack and agglomeration of GO nanosheets, which will deter ion exchange between Y(III) and H^+ to some extent and leads to a drop in Y(III) desorption rate. In summary, pH value of desorption solution is critical to high desorption rate of Y(III) on GO nanosheets.

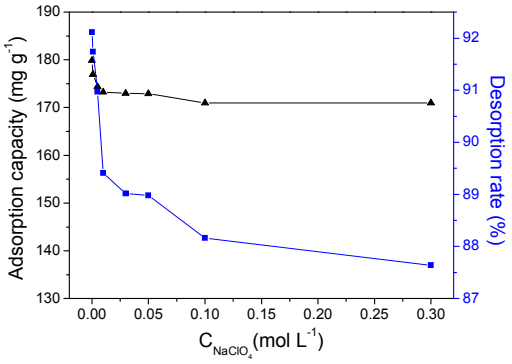

Fig. 3. Effect of ionic strength (C_{NaClO4}) on adsorption/desorption of Y(III) on GO nanosheets in colloidal suspensions.(Using $NaClO_4$ as added electrolyte, T = 303 K, adsorption time: 25 min, using pH=0.9 HNO_3 as desorbent, desorption time: 60 min)

The effects of ionic strength on adsorption and desorption of Y(III) on GO nanosheets in colloidal suspensions are presented in Fig. 3. The effect of ionic strength on desorption and adsorption of Y(III) on GO nanosheets almost demonstrates the similar evolution tendency. The variation of $NaClO_4$ concentration from 0 to 0.03 M leads to a moderate reduction of 6.91 $mg \cdot g^{-1}$ and 3.09 % in adsorption capacity and desorption rate of Y(III) on GO nanosheets, respectively. And the further increasing the $NaClO_4$ concentration from 0.03 M to 0.30 M results in a minor decrease of 1.97 $mg \cdot g^{-1}$. and 1.38 % in adsorption capacity and desorption rate, respectively. It can be interpreted as follows: (1) As the adsorption interactions between the functional groups and Y(III) ions are mainly ionic interaction, the introduction of $NaClO_4$ into GO suspension reduces the available sites to bind Y(III) ions on GO surfaces as a result of competition with Na(I); (2) When the available adsorption sites on GO surfaces are occupied by Na(I), the further enhancement of $NaClO_4$ concentration boosts the activity coefficient of Y(III) and restricts Y(III) transfer from solution to solid surface to a minor extent. [17]

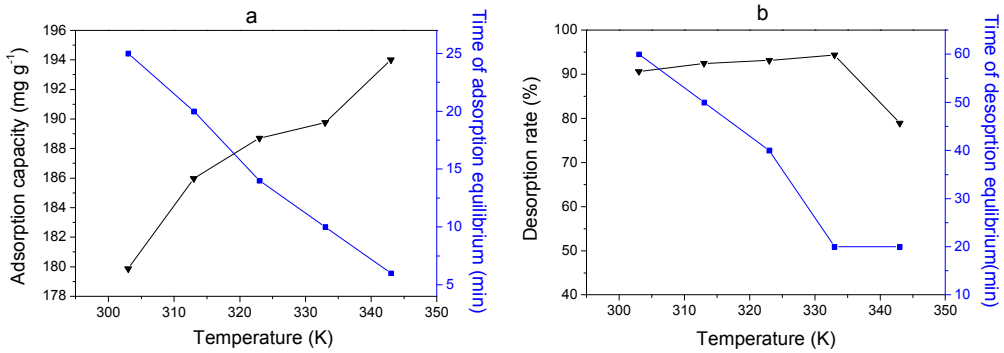

Fig. 4. Effect of temperature on adsorption (a) /desorption (b) of Y(III) on GO nanosheets. (adsorption time: 25 min, desorption time: 60 min)

The effects of temperature on adsorption and desorption of Y(III) on GO nanosheets in colloidal suspensions are shown in Fig. 4a and 4b, respectively. As the temperature increases from 303K to 343K, the time for Y(III) to reach adsorption equilibrium on GO nanosheets drastically drops from 20 min to 6 min while adsorption capacity only increases from 185.97 mg g^{-1} to 194.01 mg g^{-1} by a minor increase of 4.32%. As for the desorption of Y(III) on GO nanosheets, as the temperature increases from 303K to 333K, the time for Y(III) to reach desorption equilibrium on GO nanosheets drastically drops from 60 min to 20 min while the desorption rate climbs up tardily from 90.63% to 94.36% by a rise of 3.73%. It is noticeable that further enhancing the temperature to 343K, the time for Y(III) to reach desorption equilibrium remains unchanged while the desorption rate falls to 78.93%, which can be owing to the observed aggregation and sedimentation of GO at over 343K. It is understandable that the enhancing temperature speeds Y(III) transfer from solution to the surface of GO or the opposite.

3.3 Adsorption isotherm and thermodynamics

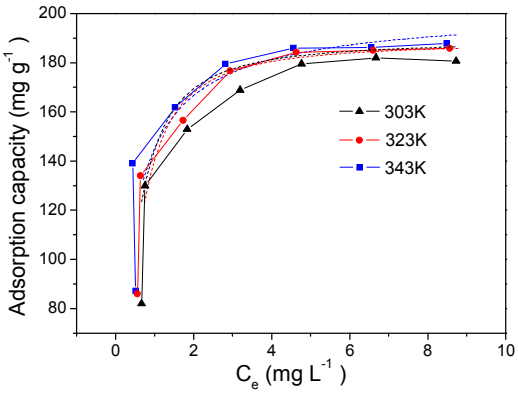

Fig. 5. Adsorption isotherms of Y(III)on graphene oxide nanosheets at different temperatures. The solid lines are adsorption model, and the dashed lines are Langmuir model simulation.

Adsorption isotherms of Y(III) on GO nanosheets at three different temperatures are shown in Fig. 5. Adsorption isotherms can be generated based on numerous theoretical models, where Langmuir and Freundlich models are the most frequently used. In order to explore the adsorption mechanism, as shown in Fig. 5, the adsorption isotherms of Y(III) on GO were simulated with the Langmuir ($C_e/q_e = C_e/q_{max}+1/q_{max}\cdot K_L$) and Freundlich ($q_e=K_F\cdot C_e^{1/n}$) models, respectively, where C_e is the equilibrium concentration of Y(III) in aqueous solution ($mg\cdot L^{-1}$), q_e is the amount of Y(III) adsorbed on colloidal GO ($mg\cdot g^{-1}$), q_{max} is the maximum amount of Y(III) adsorbed per unit weight of GO to form a complete monolayer coverage on the surface, K_L is the Langmuir adsorption equilibrium constant, which represents enthalpy of adsorption and should vary with temperature, and K_F and n is the Freundlich constants related to the adsorption capacity and adsorption intensity, respectively. The values of q_{max} and K_L are calculated from the slope and intercept of the linear plot of C_e/q_e against C_e. $\ln K_F$ and $1/n$ can be obtained from the intercept and the slope of the linear plot of $\ln q_e$ versus $\ln C_e$. The parameters calculated from Langmuir and Freundlich models are listed in Table 1.

Table 1. Parameters for Langmuir and Freundlich models of Y(III) adsorption on GO

Experimental Conditions	Langmuir			Freundlich		
	q_{max}(mg·g^{-1})	K_L(L·mg^{-1})	R^2	K_F(mg^{1-n}·L^n·g^{-1})	n	R^2
pH=5.9±0.1 T=303 K	190.48	2.59	0.9994	139.39	0.138	0.9904

As shown in Fig. S1, the Langmuir equation fits the experimental data better than the Freundlich model with a higher correlation coefficient (R^2) of 0.9994, indicating that Y(III) is adsorbed by specific site on the surface of colloidal GO sheet and forms adsorption monolayer. The maximum adsorption capacity (q_{max}) of Y(III) on GO calculated from Langmuir model is 190.48 mg·g^{-1} at pH= 5.9±0.1. Compared with q_{max} values of Y(III) adsorption on other adsorbents (Table 2), such as by-pass cement, [4] bacterial cell wall, [11] and polyethyleneglycol (phosphomolybdate and tungstate) heteropolyacid sorbents, [12] GO has the highest adsorption capacity among the reported adsorbents for Y(III) so far. This can be explained as followed: (1) The wider c-axis spacing of GO nanosheets makes Y(III) ions to enter into the interlayer space of GO nanosheets easily and be effectively bound with the abundant oxygen-containing functional groups on the surface of GO; [33] (2) Serving as Lewis base, the delocalized π electron systems can form electron donor acceptor complexes with Y(III) ions acting as Lewis acid. [17, 35]

Table 2. Comparison of maximum adsorption capacity of Y(III) on different adsorbents

Adsorbents	Experimental Conditions	Adsorption Capacity (mg·g^{-1})	Refs
by-pass cement dust	T=298K, pH =7.0 C=200 mg·L^{-1}	4	4
sulfate reducing bacteria	T=297K, pH =4.5 C=0.1 mg·L^{-1}	0.00434	11
phototorophic bacteria	T=297K, pH =4.5 C=0.1 mg·L^{-1}	0.0026	11
H,PEG, PW	T=298K, C_{HCl}=0.2 M C=400 mg·L^{-1}	55	12
H,PEG, PMo	T=298K, C_{HCl}=0.2 M C=400 mg·L^{-1}	66	12
colloidal GO	T=303K, pH =5.9±0.1 C=12 mg·L^{-1}	190.48	this study

The thermodynamic parameters (ΔH^0, ΔS^0 and ΔG^0) for Y(III) adsorption on GO

nanosheets can be calculated from the temperature-dependent adsorption isotherms. The standard free energy change (ΔG^0) can be calculated from the following equation: $\Delta G^0 = -RT\ln K^0$, where R is the universal gas constant (8.314 J·mol^{-1}·K^{-1}); T is the temperature of aqueous solution in Kelvin； The adsorption equilibrium constant, K^0, can be calculated by plotting $\ln K_d$ versus C_e (Fig. S2) and linear extrapolating C_e to zero. The standard enthalpy change (ΔH^0) and the standard entropy change (ΔS^0) are calculated according to the following equation: $\ln K^0 = \Delta S^0/R - \Delta H^0/RT$. The slope and intercept of the plot of $\ln K^0$ versus $1/T$ are $-\Delta H^0/R$ and $\Delta S^0/R$, respectively (Fig. S3).

Table 3. The thermodynamic parameters for Y(III) adsorption on GO nanosheets

ΔG^0 (kJ·mol^{-1})			ΔH^0 (kJ·mol^{-1})	ΔS^0 (J·mol^{-1}·K^{-1})
303 K	323 K	343 K		
−37.20	−40.35	−43.82	12.93	165.37

The thermodynamic parameters calculated from adsorption isotherms at 303 K, 323 K and 343 K) are listed in Table 3. The value of ΔH0 is positive, indicating that Y(III) adsorption on GO is an endothermic adsorption process. This phenomena can be explained as follows: as Y(III) ions are well solvated in aqueous solution, hydrated Y(III) ions must have their hydration sheath denuded to some extent prior to being adsorbed on graphene oxide, which is an energy-absorbing process. Based on the previous study35, the energy of dehydration exceeds the exothermicity of cation ions to be attached to graphene oxide nanosheets. It can be concluded that the dehydration of Y(III) ions is a dominant endothermic process. The negative values of ΔG0 suggest Y(III) adsorption on GO is a spontaneous process. The increase in negative values of ΔG0 with increasing temperature indicates that the higher temperature would be more favorable to adsorption of Y(III) on GO. With increasing temperature, the hydrated Y(III) ions tend to dehydrate more easily and thus the Y(III) ions adsorption on GO proceed more easily. The positive value of ΔS^0 suggests the affinity of GO toward Y(III) in aqueous solutions and the enhanced randomness for the Y(III) ions adsorption onto the active sites of GO during adsorption.

3.4 Kinetics and modeling.

The contact time between the metal ions and the adsorbent is regarded as a crucial issue in the high efficient recovery of metal ions from the wastewater via adsorption. Hence, in the present study, the kinetics of Y(III) removal by adsorption of the colloidal GO suspensions was investigated to understand the adsorption behavior of the colloidal GO suspensions.

In order to elucidate the adsorption kinetic process, two conventional pseudo-first-order and pseudo-second-order kinetic models [36, 37] have been employed to fit the experimental adsorption data in this work, which can be expressed by their nonlinear forms as follows:

pseudo-first-order model: $\ln(q_e - q_t) = \ln q_e - k_1 t$

pseudo-second-order model: $\frac{t}{q_t} = \frac{1}{k_2 q_e^2} + \frac{t}{q_e}$

Where k_1 (min^{-1}) and k_2 ($\text{mg}\cdot\text{g}^{-1}\cdot\text{min}^{-1}$) are the adsorption rate constants of the pseudo-first-order model and pseudo-second-order model, respectively; q_e is the actual equilibrium adsorption capacity of adsorbent ($\text{mg}\cdot\text{g}^{-1}$); q_t is the actual adsorption capacity of adsorbent after contacting for t minutes ($\text{mg}\cdot\text{g}^{-1}$).

The plots of kinetic models of pseudo-first-order and pseudo-second-order for Y(III) adsorption on GO nanosheets are presented in Fig. 6a, and the parameters for the two kinetic models are summarized in Table S1. Fig. 6a shows that the adsorption kinetic can be perfectly fitted by the pseudo-second-order model with correlation coefficient R^2=0.9982, suggesting that the adsorption process follows pseudo-second-order model.

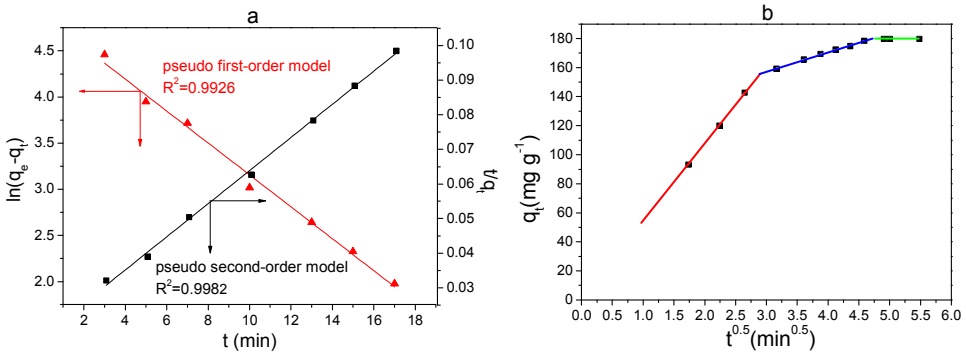

Fig. 6. (a) Kinetic models of pseudo-first-order and pseudo-second-order; (b) Intraparticle diffusion kinetics for Y(III) adsorption on GO nanosheets

In generally, adsorption process consists of three consecutive steps, namely (a) external diffusion (surface adsorption); (b) intraparticle diffusion (pore diffusion); and (c) the final adsorption equilibrium on active site.[38] The final step is relatively very fast. Therefore, the sorption of adsorbate on sorbent may be governed by film diffusion process and/or intraparticle diffusion.. To elucidate the diffusion mechanism and determine the actual rate-controlling step, regression analysis was carried out for the plot of the Y(III) adsorbed amount (q_t) versus the square root of time ($t^{0.5}$) according to Weber–Morris' intraparticle diffusion model, $q_t = k_p t^{0.5} + C$,[39] where k_p is the intraparticle diffusion constant (mg·g^{-1}·min$^{-0.5}$), C gives an idea about the thickness of the boundary layer. Based on the model, if the plot passes through the origin (C=0), it indicates that the intraparticle diffusion is only rate-controlling step; if the plot does not pass through the origin(C≠0), this suggests that not only the intraparticle diffusion is rate-controlling step, but also other kinetic processes may control the adsorption rate simultaneously. As shown in Fig. 6b, the plot of q_t versus $t^{1/2}$ has three distinct regions, suggesting that more than one process dominates the adsorption. The first sharper region represents external diffusion and covers most of adsorption period, which might be due to the reason that confinement of GO in dialysis bag prolongs ion diffusion distance and enhances ion diffusion hindrance. The second region is the gradual adsorption stage, which corresponds to intraparticle diffusion. The third region suggests adsorption-desorption equilibrium. Apparently, the plot does not pass through the origin, indicating that the intraparticle diffusion is

not the only rate controlling step for the adsorption process. Similar adsorption behavior was observed by Y.M. Ren et al.[40] in the adsorption of copper and lead ions onto graphene nanosheet/δ-MnO_2

3.5. Recycling and regeneration of colloidal graphene oxide suspensions

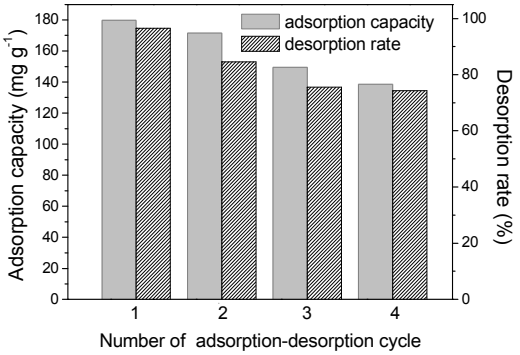

Fig. 7. Histograms for the adsorption capacity (q_e) and desorption rate (R_d) of Y(III) on colloidal GO suspensions in consecutive adsorption-desorption cycles

It is well-known to us that an ideal adsorbent should not only possess high adsorption/desorption capability, but also have excellent reusability from the viewpoint of economy and applicability. Considering the regeneration ability of the GO is highly crucial to its practical application, the experiments of consecutive adsorption-desorption cycle were conducted by using GO suspension loaded in dialysis bag as adsorbent and pH=0.90 M HNO_3 aqueous solution as desorption agent to investigate the desorption and adsorption behaviors of the GO.

From Fig. 7, it can be seen that the desorption rate in the fourth adsorption -desorption cycle still retains 74.26%, suggesting that most Y(III) adsorbed on the surface of the GO could be desorbed using pH=0.90 HNO_3 aqueous solution. More significantly, Fig. 7 indicates that GO still preserves the adsorption capacity of 138.73 mg g^{-1} by reduction of 22.92% after the three consecutive adsorption-desorption cycles. The decreasing adsorption capacity of GO after several adsorption-desorption cycles suggests that there are a fraction of the sites that are irreversibly bound by Y(III). The reason may be that with the growing adsorption-desorption cycles, the restack of GO nanosheets intensifies, which makes Y(III) ions desorption more difficult and exposes less active sites available for adsorption. As to the inset in Fig.

2b, the precipitated GO nanosheets suspension after adsorption saturation can resume colloidal state when using pH=0.90 HNO_3 aqueous solution as desorption agent. Therefore, the high adsorption capacity and desorption rate of the colloidal GO indicates the regenerability and reusability of the GO and promises a vast application prospect of GO in practical waste water treatment.

4. Conclusions

Herein, a novel and re-pollution-free route for highly efficient recovery of trace Y(III) from wastewater by adsorption of aqueous colloidal suspension of GO loaded in dialysis bag has been proposed. At pH=5.9±0.1 and T=303 K, the adsorption capacity of Y(III) on colloidal GO nanosheets can amount up to 190.48 $mg \cdot g^{-1}$ after 25-minite adsorption higher than any other adsorbents reported so far. The Y(III)-saturated GO suspension can be easily desorbed and resume colloidal state in pH= 0.90 HNO_3 solution with desorption rate of 74.26% in the fourth adsorption -desorption cycle. In summary, GO nanosheets may act as a highly efficient and easily regenerable adsorbent in enrichment and recovery of trace Y(III) from wastewater. More significantly, the innovative combination of colloidal GO suspension with dialysis membrane offers a facile and feasible strategy for re-pollution-free adsorptive separation and recovery of other metal ions from wastewater.

Acknowledgements

We are grateful for financial support from the Project in the National Science & Technology Pillar Program of China (2012BAE01B02), National Natural Science Foundation of China (No.51464033 and No.21061011) and Jiangxi Provincial Scientific & Technological Support Project of China (No. 20132BBE500041)

References

1. R. Chi and J. Tian, *Weathered crust elution-deposited rare earth ores*. Nova

Science Publishers, New York, 2008.

2. S. L. Tong, W. Z. Zhu, Z. H. Gao, Y. X. Meng, R. L. Peng and G. C. Lu, *J. Environ. Sci. Hea. A*, 2004, **39**, 2517 −2532.
3. C. R. Li, Z. Y. Zhuang, F. Z. Huang, C. Wu, Y. P. Hong and Z. Lin, *ACS Appl. Mater. Interfaces*, 2013, **5**, 9719−9725.
4. H. H. Osman, S. A. Sayed and M. E. H. Shalabi, *J. Hazard. Mater.*, 2011, **195**, 62–67.
5. M. R. Yaftian, M. Burgard, C. B. Dieleman and D. Matt, *J. Membr. Sci.*, 1998, **144**, 57–64.
6. R. Chi, Y. Hu, G. Zhu, S. Xu, Z. Zhou and Z. Xu, *Metal. Mater. Trans. B.*, 2003, **34**, 611−617.
7. S. P. Dubey, K. Gopal and J. L. Bersillon, *J. Environ. Biol.*, 2009, **30**, 327−332.
8. K. C. Kemp, H. Seema, M. Saleh, N. Le, K. Mahesh, V. Chandra and K. Kim, *Nanoscale*, 2013, **5**, 3149−3171.
9. H. M. H. Gad and N. S. Awwad, *Sep. Sci. Technol.*, 2007, **42**, 3657−3680.
10. Y. Takahiro, O. Takuo, O. Toshihiko and J. F. Arokiasamy,. *Chem. Geol.*, 2004, **21**, 239–246.
11. Y. Takahashi, X. Châtellier, K. H. Hattori, K. Kato and D. Fortin, *Chem. Geol.*, 2005, **219**, 53–67.
12. L. Zhang, S. D. Ding, T. Yang and G. C. Zheng, *Hydrometallurgy*, 2009, **99**, 109–114.
13. S. B. Wang, H. Q. Sun, H. M. Ang and M. O. Tadé, *Chem. Eng. J.*, 2013,**226**, 336–347.
14. R. D. Daniel, P. Sungjin, W. B. Christopher and S. R. Rodney, *Chem. Soc. Rev*. 2010, **39**, 228–240.
15. D. Li, M. Marcb, E. Scottgilj, K. Richardb and G. W. Gordon, *Nat. nanotechnol*.,

2008, **3**, 101– 105.

16. R. Sitko, E. Turek, B. Zawisza, E. Malicka, E. Talik, J. Heimann, A. Gagor, B. Feist and R. Wrzalik, *Dalton Trans*., 2013, **42**, 5682–5689.
17. G. X. Zhao, J. X. Li, X. M. Ren, C. I. Chen and X. K. Wang, *Environ. Sci. Technol.*, 2011, **45**, 10454–10462.
18. G. X. Zhao, X. M. Ren, X. Gao, X. L. Tan, J. X. Li, C. I. Chen, Y. Y. Huang and X. K. Wang, *Dalton Trans.*, 2011, **40**, 10945–10952.
19. G. X. Zhao, T. Wen, X. Yang, S. B. Yang, J. L. Liao, J. Hu, D. D. Shao and X. K. Wang, *Dalton Trans.,* 2012, **41**, 6182–6188.
20. Y. B. Sun, Q. Wang, C. I. Chen, X. L. Tan and X. K. Wang, *Environ. Sci. Technol.*, 2012, **46**, 6020−6027.
21. Z. Q. Bai, Z. J. Li, C. Z. Wang, L. Y. Yuan, Z. R. Liu, J. Zhang, L. R. Zheng, Y. L .Zhao, Z. F. Chai and W. Q. Shi, *RSC Adv.*, 2014, **4**, 3340–3347.
22. J. Yang, J. X. Wu, Q. F. Lü and T. T. Lin, *ACS Sustainable Chem. Eng.*, 2014, **2**, 1203 −1211.
23. Y. B. Sun, D. D. Shao, C. L. Chen, S. B. Yang and X. K. Wang, *Environ. Sci. Technol.*, 2013, **47**, 9904−9910.
24. X. L. Wu, L. Wang, C. L. Chen, A. W. Xu and X. K. Wang, *J. Mater. Chem.*, 2011, **21**, 17353–17359
25. V. Chandra, J. Park, Y. Chun, J. W. Lee, I.C. Hwang and K. S. Kim, *ACS .Nano.*, 2010*,* **4**, 3979–3986.
26. J. H. Zhu, S.Y. Wei, H.B. Gu, S. B. Rapole, Q. Wang, Z.P. Luo, N.

Haldolaarachchige, D. P. Young and Z.H. Guo, *Environ. Sci. Technol.*, 2012, **46**, 977−985

27. L. L. Fan, C. N. Luo, M. Sun and H. M. Qiu, *J. Mater. Chem.*, 2012, **22**, 1039–1046.
28. H. M. Sun, L.Y. Cao and L. H. Lu, *Nano. Res*., 2011, **4**, 550–562.
29. J. Li, S. W. Zhang, C. L. Chen, G. X. Zhao, X. Yang, J.X. Li and X. K. Wang, *ACS Appl. Mater. Interfaces*, 2012, **4**, 4991−5000
30. L. Zhang, X. Li, Y. Huang, Y. F. Ma, X. J. Wan and Y. S. Chen, *Carbon*, 2010, **48**, 2367–2371.
31. C. M. Chen, Q. H. Yang, Y. G. Yang, W. Lv, Y.F. Wen, P. X. Hou, M. Z. Wang and H. M. Cheng, *Adv. Mater.*, 2009*,* **21**, 3007–3011.
32. D. C. Marcano, D. V. Kosynkin, J. M. Berlin, A. Sinitskii, Z. Z. Sun, A. Slesarev, L. B. Alemany, W. Lu and J. M. Tour, *ACS Nano.*, 2010, **4**, 4806–4814.
33. M. J. McAllister, J.L. Li, D. H. Adamson, H. C. Schniepp, A. A. Abdala, J. M. Liu,; M. Herrera-Alonso, D. L Milius,. R. Car, R. K. Prud' homme and I. A. Aksay, *Chem. Mater.*, 2007, **19**, 4396–4404.
34. K. N. Kudin, B. Ozbas, H.C. Schniepp, R.K. Prud' homme, I.A. Aksay and R. Car, *Nano Lett.*, 2008, **8**, 36–41.
35. C. Laurence and J. F. Gal, *Lewis Basicity and Affinity Scales: Data and Measurement*, Wiley, New York, 2009.
36. C. W. Hoogendam, A. De Keizer, M. A. Cohen Stuart and B. H. Bijsterbosch, *Langmuir*, 1998, **14**, 3825–3839.
37. Y. Liu and L. Shen, *Langmuir*, 2008, **24**, 11625–11630.
38. N. Li, Z. Mei and X. Y. Wei, *Chem. Eng. J.*, 2012, **192**, 138–145.

39. W. J. Weber and J. C. Morris, *J. San. Eng. Div.*, 1963, **89**, 31–59.

40. Y. M. Ren, N. Yan, J. Feng, J. Ma, Q. Wen, N. Li and Q. Dong,. *Mater. Chem. Phys.*, 2012, **136**, 538–544.